Effects of 5*d* electrons and spin-orbit interaction on the characteristics of bulk plasmons in lead

X. Zubizarreta,[1,2,3] V. M. Silkin,[1,2,4] and E. V. Chulkov[1,2,5]

[1]*Donostia International Physics Center (DIPC), Paseo de Manuel Lardizabal 4, 20018 San Sebastián/Donostia, Basque Country, Spain*

[2]*Departamento de Física de Materiales, Facultad de Ciencias Químicas, Universidad del País Vasco/Euskal Herriko Unibertsitatea, Apdo. 1072, 20080 San Sebastián/Donostia, Basque Country, Spain*

[3]*Max-Planck-Institut für Mikrostrukturphysik, Weinberg 2, 06120 Halle, Germany*

[4]*IKERBASQUE, Basque Foundation for Science, 48011 Bilbao, Spain*

[5]*Centro de Física de Materiales CFM - Materials Physics Center MPC, Centro Mixto CSIC-UPV/EHU, Paseo de Manuel Lardizabal 5, 20018 San Sebastián/Donostia, Basque Country, Spain*

(Received 7 April 2014; revised manuscript received 18 August 2014; published 15 October 2014)

An *ab initio* study of the dynamical dielectric response of bulk lead is presented. The influence of the 5*d* semicore states on the characteristics of the bulk plasmon is analyzed by means of first-principles pseudopotential calculations. The effects of spin-orbit interactions and local-fields are also studied in detail. The inclusion of the 5*d* semicore states in the valence configuration completely changes the high-energy-transfer dielectric properties of bulk Pb. In particular, it lowers the computed bulk plasmon energy by about 3.5 eV, bringing its frequency to good agreement with experimental data. In general, the high-energy-transfer dielectric response of bulk Pb is found to be shaped mostly by the interplay between the interband transitions involving the semicore 5*d* states and the spin-orbit coupling interaction. Local-field effects are found to affect the relative spectral weight of the high-energy excitations, while leaving their dispersion mostly unaffected.

DOI: 10.1103/PhysRevB.90.165121 PACS number(s): 71.20.Be, 71.45.Gm

I. INTRODUCTION

The study of collective electronic excitations (plasmons [1]) involving valence electrons in solids has lasted more than a half century and represents an active field of current interest for many researchers. From the theoretical side, the first-principles calculations constituted a solid background for obtaining reliable results that can be directly compared with experiment data. Since information about the electronic structure of a material is known from band-structure calculations, e.g., derived within the Kohn–Sham density-functional approach, the calculated spectra often reproduce experimental data with high accuracy. However, in such an approach one should consider several factors that might play an important role in a given system. One of these factors is the effect of exchange-correlations on the excitation spectra beyond the random-phase approximation (RPA) when interactions between the excited electron and hole are neglected. This effect was considered in detail and several approximations for its inclusion were proposed. It constituted an attractive topic in the studies based on a free-electron-gas model used to simulate the band structure of solids [2–7]. Within an *ab initio* approach it was also demonstrated that, e.g., the time-dependent local-density approximation (TDLDA) gives a significantly better description of excitation spectra at finite momentum transfer, as was shown for materials like Si [8], transition metals [9], and Al [10].

Numerous studies also demonstrated the importance of local-field effects [11,12] (LFEs), which are related to the spatial inhomogeneity in real crystals. In particular, LFEs have dramatic impact on reflectivity and absorbance in the far-UV range [13,14]. Spectacular manifestation of the LFE was observed in MgB_2 where the spectral weight of the intraband plasmon [15,16] is transferred from small momentum transfer q to large q's in the successive Brillouin zones (BZs) leading to a remarkable cosine-like plasmon dispersion [17]. Reappearance of a plasmon mode at large q caused by the LFEs was also found in graphite [18], compressed lithium [19], and transition metals dichalcogenides [20,21].

It is also known that the band structure can be strongly influenced by spin-orbit (SO) effects, especially in materials composed of heavy elements. Remarkable examples are lead, bismuth, bismuth tellurohalides, and topological insulators [22,23] whose electron band structure, vibrational spectra, and the electron-phonon interaction are strongly modified by the SO coupling [24–30]. Since the electronic structure of heavy elements notably depends on relativistic effects, one may expect the corresponding impact on the excitation spectrum. Nevertheless, although the relativistic effects on the electronic structure were studied in great detail, respective calculations of dielectric properties from first-principles were performed in only a few cases. In particular, it was demonstrated that the SO interaction induces sizable effects in the dielectric properties of Pb [31,32].

The presence of several energy bands in real materials leads to two types of transitions: intraband transitions (within the energy bands crossing the Fermi level) and numerous interband transitions between different occupied and unoccupied bands. Very often, these transitions play an important role in the formation of excitation spectrum; in particular, of plasmon properties. For instance, the intraband transitions within several partly occupied energy bands induce low-energy plasmons with characteristic sound-like dispersion in some materials [20,21,33–35]. The interband transitions give rise to a strong redshift of the Ag plasmon frequency [36,37] or to a negative momentum dispersion [38,39] of the plasmon in heavy alkali metals [40,41]. Moreover, these transitions dominate the energy-loss landscape in the low-energy-transfer domain in many materials like MgB_2 [15,16], intercalated graphite [35,42], transition-metal dichalcogenides [20,21,43–45], lead [31], and Heusler compounds [46].

Since the distinction between core and valence electrons is blurred for several elements of the periodic table, the number of the valence orbitals must be increased in some cases, depending not only on the atomic species but also on the precise physical property under consideration. As an example, the semicore $3d$ electrons of gallium are usually treated using a so-called nonlinear core correction [47]. Excitations from the semicore states shift the optical absorption band to higher energies by several eV [13,14]. Also, the inclusion of the $3s$ and $3p$ electrons of titanium in the valence configuration leads to a different theoretical crystal structure [48]. It was also demonstrated that, in some cases, it is important to take into account the lifetime effects to obtain qualitatively correct spectra [49,50].

A goal of the present study is to analyze the dynamical dielectric response of bulk lead, demonstrating that it is mainly the result of the interplay between transitions involving the $5d$ electrons, SO effects, and, of minor importance, local-field effects. Here we focus on the dynamics of the bulk plasmon and on higher-energy features. First, the energy of the $5d$ states of Pb is discussed. Next, their role on the dielectric response is shown both in the long-wavelength regime and for finite values of momentum transfer. Additionally, the SO coupling effects, LFE, and possible anisotropy effects are analyzed. The calculations have been done using the first-principles pseudopotential approach within the time-dependent density functional theory (TDDFT) [51,52] taking explicitly into account the $5d$ states.

The rest of the paper is organized as follows: In Sec. II details of the calculation method employed in this study are presented, while in Sec. III the electronic structure of bulk lead, the SO coupling effects, and the energy position of the $5d$ electrons are discussed. Section IV shows the effect of the semicore $5d$ electrons on the dielectric response of lead, together with a comparison with available experimental data and other theoretical results. In Sec. V the general results for the dynamical dielectric response and the role of different factors are analyzed in detail. Finally, the main conclusions are drawn in Sec. VI. Unless otherwise stated, atomic units are used throughout, i.e., $e^2 = \hbar = m_e = 1$.

II. CALCULATION METHOD

Information on collective electronic excitations of the valence electrons of a system can be extracted from the peaks of the energy-loss function, defined as the imaginary part of the inverse macroscopic dielectric function, $\mathrm{Im}[\epsilon_{\mathrm{M}}^{-1}]$. This quantity is proportional, within the first Born approximation, to the inelastic scattering cross section of x rays and electrons [1] measured in experiments like inelastic x-ray scattering spectroscopy and electron energy-loss spectroscopy.

In the case of a periodic solid, the Fourier coefficients of the energy-loss function $L(\mathbf{Q},\omega)$ at a certain momentum transfer $\mathbf{Q}$ and energy ω are defined by the diagonal part of the $\mathrm{Im}[\epsilon^{-1}_{\mathbf{GG}'}(\mathbf{q},\omega)]$ matrix related to the density-response function for interacting electrons $\chi(\mathbf{r},\mathbf{r}',\omega)$ through

$$\epsilon^{-1}_{\mathbf{GG}'}(\mathbf{q},\omega) = \delta_{\mathbf{GG}'} + v_{\mathbf{G}}(\mathbf{q})\chi_{\mathbf{GG}'}(\mathbf{q},\omega), \tag{1}$$

with $v_{\mathbf{G}}(\mathbf{q}) = 4\pi|\mathbf{q}+\mathbf{G}|^{-2}$ being the Fourier transform of the bare Coulomb interaction. Here $\mathbf{G}$ is the reciprocal lattice vector and $\mathbf{Q} = \mathbf{q} + \mathbf{G}$ with $\mathbf{q}$ restricted to the first Brillouin zone.

In the framework of TDDFT [51,52], the density-response function χ in Eq. (1) satisfies the matrix equation

$$\chi_{\mathbf{GG}'}(\mathbf{q},\omega) = \chi^{\mathrm{o}}_{\mathbf{GG}'}(\mathbf{q},\omega) + \sum_{\mathbf{G}_1}\sum_{\mathbf{G}_2}\chi^{\mathrm{o}}_{\mathbf{GG}_1}(\mathbf{q},\omega) \times \left[v_{\mathbf{G}_1}(\mathbf{q})\delta_{\mathbf{G}_1\mathbf{G}_2} + K^{\mathrm{XC}}_{\mathbf{G}_1\mathbf{G}_2}(\mathbf{q})\right]\chi_{\mathbf{G}_2\mathbf{G}'}(\mathbf{q},\omega), \tag{2}$$

where $\chi^{\mathrm{o}}_{\mathbf{GG}'}(\mathbf{q},\omega)$ is the matrix of the Fourier coefficients of the density-response function for noninteracting Kohn–Sham electrons. $K^{\mathrm{XC}}_{\mathbf{GG}'}(\mathbf{q})$ stands for the Fourier components of the exchange-correlation (XC) kernel, whose exact form is unknown. Several approximations to K^{XC} were proposed [53–55]. Here we employ two frequently used approximations: RPA when one simply sets K^{XC} to zero and TDLDA [54].

In order to save computational time, instead of a direct evaluation of the real and imaginary parts of the $\chi^0_{\mathbf{GG}'}(\mathbf{q},\omega)$ matrix, we calculate first the spectral function matrix $S^0_{\mathbf{GG}'}(\mathbf{q},\omega)$ by using the following expression [56,57]:

$$S^0_{\mathbf{GG}'}(\mathbf{q},\omega) = \frac{1}{\Omega}\sum_{\mathbf{k}}^{1\mathrm{BZ}}\sum_{n}^{\mathrm{occ}}\sum_{n'}^{\mathrm{unocc}}\delta(\varepsilon_{n\mathbf{k}} - \varepsilon_{n'\mathbf{k}+\mathbf{q}} + \omega) \times \langle\psi_{n\mathbf{k}}|e^{-\mathrm{i}(\mathbf{q}+\mathbf{G})\cdot\mathbf{r}}|\psi_{n'\mathbf{k}+\mathbf{q}}\rangle\langle\psi_{n'\mathbf{k}+\mathbf{q}}|e^{\mathrm{i}(\mathbf{q}+\mathbf{G}')\cdot\mathbf{r}}|\psi_{n\mathbf{k}}\rangle. \tag{3}$$

In Eq. (3), n and n' are band indices, wave vectors $\mathbf{k}$ are in the first BZ, and $\varepsilon_{n\mathbf{k}}$ and $\psi_{n\mathbf{k}}$ are Bloch eigenvalues and eigenfunctions, respectively, of the Kohn–Sham Hamiltonian. From the knowledge of $S^0_{\mathbf{GG}'}(\mathbf{q},\omega)$, the imaginary part of $\chi^0_{\mathbf{GG}'}(\mathbf{q},\omega)$ is readily evaluated through the relation

$$S^0_{\mathbf{GG}'}(\mathbf{q},\omega) = -\frac{1}{\pi}\mathrm{sgn}(\omega)\mathrm{Im}\left[\chi^0_{\mathbf{GG}'}(\mathbf{q},\omega)\right], \tag{4}$$

where $\mathrm{sgn}(\omega) = 1$ (-1) for $\omega > 0$ $(\omega < 0)$. The real part of $\chi^0_{\mathbf{GG}'}(\mathbf{q},\omega)$ is obtained numerically from the corresponding imaginary part by using the Hilbert transform.

Inclusion of the $\mathbf{G} \neq \mathbf{G}'$ matrix elements in Eq. (2) couples the contributions corresponding to different reciprocal lattice vectors $\mathbf{G}$ and $\mathbf{G}'$. In general, this leads to a deviation of the macroscopic $\epsilon_{\mathrm{M}}(\mathbf{Q},\omega)$ from the microscopic dielectric function $\epsilon(\mathbf{Q},\omega) = \epsilon_{\mathbf{GG}}(\mathbf{q},\omega)$ at $\mathbf{Q} = \mathbf{q} + \mathbf{G}$. This coupling represents the so-called crystalline local-field effects [11,12] which can be notable if there is significant spatial variation in the valence electron density of the system.

In the present ground-state density-functional-theory (DFT) calculations, the electron-ion interaction is described by a norm-conserving nonlocal pseudopotential [58] and the exchange-correlation potential is described within the local-density approximation (LDA) with the use of the Perdew–Zunger [59] parametrization of the XC energy of Ceperley and Alder [60]. Well-converged results for the face-centered cubic (fcc) bulk Pb with the experimental lattice constant of 4.95 Å have been obtained with a kinetic-energy cutoff of 14 Ry (40 Ry), including ∼180 (∼880) plane waves in the expansion of the Bloch states when the $5d$ electrons were included in the core (valence) configuration. The band structure calculations were performed with inclusion of the SO term in the Hamiltonian fully self-consistently. In the

evaluation of $S^0_{GG'}(\mathbf{q},\omega)$, the SO coupling enters Eq. (3) through the energy spectrum (the δ function) and coupling matrices (the brackets).

Two different sets of calculations were carried out in evaluating Eq. (3). First, when using the scalar-relativistic one-electron energies and wave functions, $S^0_{GG'}(\mathbf{q},\omega)$ was calculated with a $144 \times 144 \times 144$ Monkhorst–Pack grid [61] of $\mathbf{k}$ wave vectors for the BZ sampling. The broadening of the Gaussian that modeled the energy-conserving Dirac delta function was fixed to be 50 meV [see Eq. (3)], while the energy-transfer mesh step is $\Delta\omega = 40$ meV. In the SO-included case, a coarser $48 \times 48 \times 48$ mesh was employed in evaluating Eq. (3) when two-component spinors represented the wave functions. The broadening of the modified Gaussian ensuring energy conservation was fixed at 150 meV, while the energy-transfer mesh step was $\Delta\omega = 20$ meV. In both sets of calculations up to 50 plane waves were employed in the expansion of the density-response and dielectric function matrices.

III. SEMICORE ELECTRONS OF LEAD AND BULK BAND STRUCTURE

As stated in the introduction, the distinction between core and valence electrons is rather ambiguous for several elements in the periodic table. In the case of Pb, the 5*d* states are usually considered as belonging to the core levels upon construction of pseudopotentials to model the electron-ion interaction. In Fig. 1 we illustrate schematically the binding energies of the semicore 5*d* electrons of atomic, bulk, and surface lead. Note the big SO splitting between the $5d_{5/2}$ and $5d_{3/2}$ levels. In the solid this splitting is reduced and both levels (transformed into bands) shift upward. In atoms located at the surface

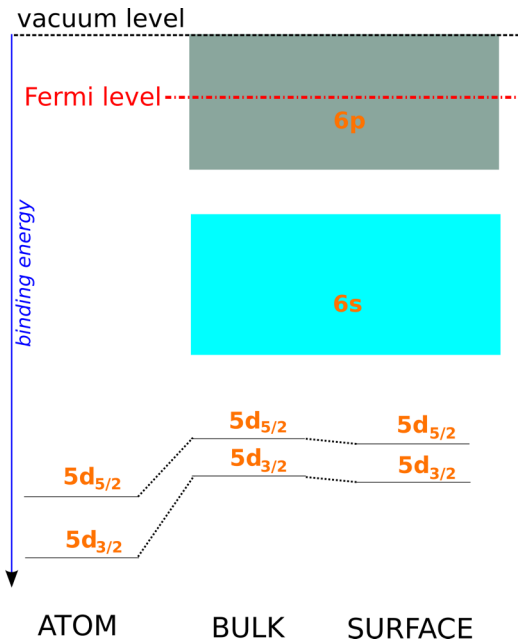

FIG. 1. (Color online) Schematic representation of the binding energy of the semicore 5*d* electrons of lead in the atom, bulk, and surface. The colored rectangles represent the 6*s*- and 6*p*-like energy bands in bulk Pb, with a finite bandwidth. For simplicity the bulk and surface Fermi levels (E_F) are considered to be equal.

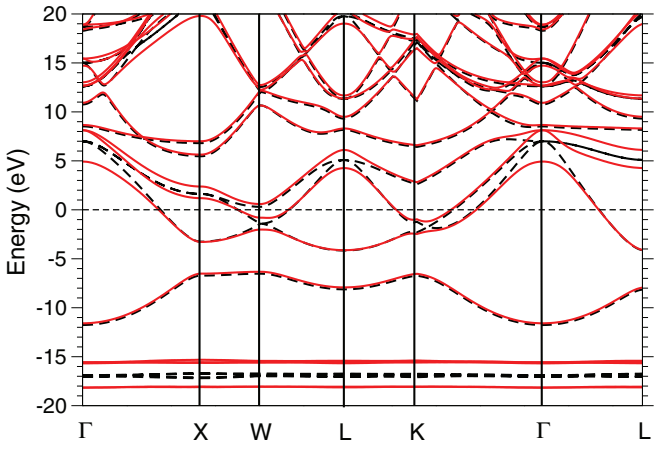

FIG. 2. (Color online) Electronic band structure of bulk lead, calculated with (red solid lines) and without (black dashed lines) spin-orbit interaction included. The 5*d* semicore electrons are considered in the valence configuration, their corresponding energy bands are located at energies below -15 eV. The horizontal thin dashed line represents the Fermi level set to zero.

the splitting slightly increases and the levels shift down in comparison with ions located inside the solid. In principle, such shifts of binding energies of the 5*d* electrons in the solid and at the surface open the possibility to find effects arising from the semicore 5*d* states in the dynamics of plasmonic excitations of lead in its different solid forms.

Figure 2 shows the calculated band structure of bulk lead along some high-symmetry directions of the first BZ evaluated with (solid lines) and without (dashed lines) inclusion of the SO interaction in the Hamiltonian. The calculated band structure with the SO term included is in good agreement with other calculations (see, e.g., Refs. [26,27]) and with the experimental one [62]. As can be seen in Fig. 2, the SO interaction causes sizeable effects on the *p*-like bands crossing the Fermi level, mainly around the high-symmetry points of the BZ. It was shown that these modifications in the electronic structure produce significant effect on the low-energy excitation spectrum of lead [31].

Another consequence of the inclusion of the SO term is the splitting of the 5*d* bands, located at $\sim$17 eV below the Fermi level at the scalar-relativistic level, into the $5d_{5/2}$ and $5d_{3/2}$ bands located, respectively, at energies ~ -15.5 and ~ -18 eV. Note that the rest of the valence *s*- and *p*-like bands remains unchanged upon inclusion of the 5*d* electrons into the valence states. The electronic structure of bulk Pb shown in Fig. 2 is in good agreement with a recent theoretical study [26] in which the same theoretical framework was used in obtaining the band structure of bulk Pb. In particular, the semicore states in Ref. [26] were found at the same energies as reported in the present work.

IV. SEMICORE EFFECTS ON DIELECTRIC RESPONSE

A. Optical limit

In Fig. 3 we compare the calculated results for the dielectric function and energy-loss function of bulk Pb obtained in the long-wavelength limit ($q \to 0$) with the data of reflectance

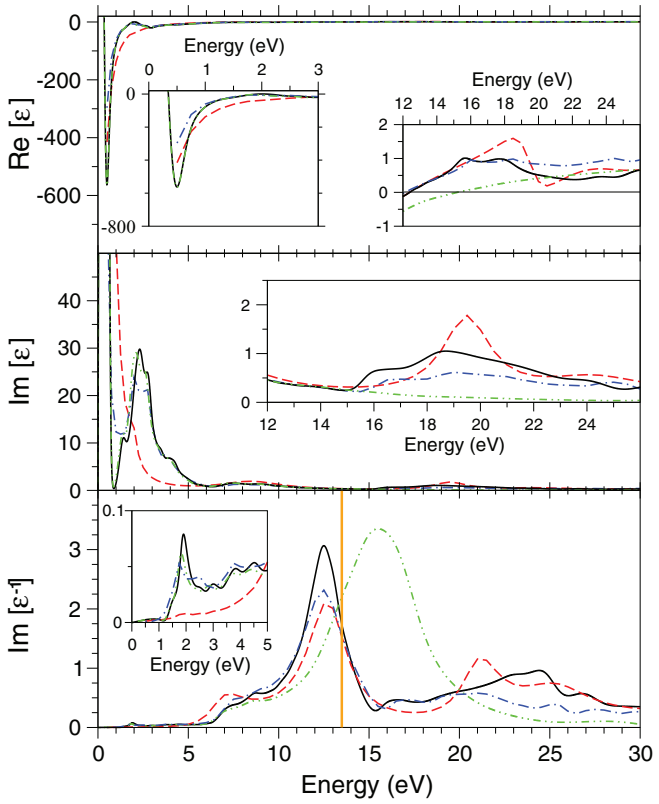

FIG. 3. (Color online) Comparison of the present results at $q \to 0$ with the data reported in Ref. [63]. Top panel: real part of the dielectric function. Middle panel: imaginary part of the dielectric function. Bottom panel: energy-loss function. The black solid (green dashed-dotted-dotted) curves represent the results obtained in the present work with the semicore electrons included in the valence (core) configuration. The red dashed and blue dashed-dotted curves stand for the experimental and theoretical results, respectively, of Ref. [63]. The insets are zooms into relevant ω ranges (see text). The vertical orange line in the bottom panel represents the free-electron-gas (FEG) plasmon energy of $\omega_p^{\mathrm{FEG}} \simeq 13.5$ eV.

electron energy-loss spectroscopy (REELS) experiment [63]. Here we also report the results of the all-electron (the $5d$ electrons are explicitly taken into account) DFT-RPA calculations using a different scheme [64] both for the ground state and the linear-response calculations reported in the same work [63]. As can be seen in the bottom panel of Fig. 3, a wide plasmon peak centered at energy of 16 eV is observed in the dash-dot-dot line representing the energy-loss function evaluated when the semicore electrons are excluded from the dielectric response calculations. Such plasmon energy is in significant disagreement with the experimental value of 12.7 eV. Note that this result is independent of the XC kernel type used and of incorporation of LFEs. Moreover the plasmon peak width is about 4 eV, i.e., about two times bigger than the one measured in the REELS experiment [63].

However, once the $5d$ bands are explicitly taken into account, the plasmon peak is shifted downward by about 3.5 eV and centered at the energy of 12.5 eV. This value for plasmon energy in lead is in excellent agreement with an experimental value of 12.7 eV and $\omega_p = 12.6$ eV extracted from the all-electron calculations of Ref. [63]. To show the level of uncertainty in the experimental determination of the plasmon energy in lead we would like to mention $\omega_p = 13.25 \pm 0.2$ eV measured in a previous energy-loss experiment [65]. This significant downward shift of the plasmon peak in the energy-loss function can be related to the fact that the interband transitions between the $5d$ bands and the lowest unoccupied states significantly enhance $\mathrm{Im}[\epsilon]$ above 15.5 eV as follows from comparison of the black solid line and the green dash-dot-dot line in the inset of the middle panel of Fig. 3.

This enhancement in $\mathrm{Im}[\epsilon]$ is accompanied by the corresponding changes in the real part of the dielectric function. Thus, from comparison of the black solid (obtained with the $5d$ states as valence electrons) and the green dashed-dotted-dotted (obtained with the $5d$ states belonging to the core) curves in the inset of the top panel of Fig. 3 one can observe the lowering by $\sim$2.7 eV of the energy at which $\mathrm{Re}[\epsilon]$ reaches zero upon inclusion of the semicore $5d$ electrons. Together with the presence of a shallow local minimum in $\mathrm{Im}[\epsilon]$ at energies just below 15.5 eV this ensures a well-defined peak in the energy-loss function around 12.5 eV corresponding to a plasmon mode.

Besides of a general agreement with the results of Ref. [63], some differences can be noted in Fig. 3. Thus the plasmon peak in the energy-loss function derived here is about 30% higher with respect to both experimental and theoretical results reported in Ref. [63]. This difference can be understood in the following terms:

First, by comparing the black solid line with the blue dash-dot and red dash curves in the inset of the middle panel of Fig. 3 one can observe that the onset in $\mathrm{Im}[\epsilon]$ for the interband transitions involving the $5d$ electrons of Pb is located at lower energies by $\sim$0.5 eV in the present pseudopotential calculations in comparison with both the calculation and experiment of Ref. [63]. This may signal that, in the present calculations, the binding energy of the $5d$-derived energy bands is underestimated by this value. Since the same binding energy for these bands was obtained in an independent pseudopotential calculation [26], this may reveal a problem of the pseudopotential approach in describing the energy position of these bands. On the other hand, this difference is comparable with the experimental uncertainty in the determination of the energy position of the $5d$ bands. Thus, in reflectance measurements reported in Ref. [66], two peaks in $\mathrm{Im}[\epsilon]$ observed at 18.7 and 21.5 eV were assigned to transitions between the $5d_{5/2}$ and $5d_{3/2}$ semicore levels and the Fermi surface. These values differ notably from the peak positions in $\mathrm{Im}[\epsilon]$ of Ref. [63].

Second, neglecting the LFEs we find that the height of the calculated plasmon peak is very close to that of Ref. [63]. Indeed we observed that the LFEs cause some spectral weight transfer to the main plasmon of 12.5 eV from the broad feature located in the 20 to 25 eV energy interval as can be appreciated from comparison of the middle and left panel columns of Fig. 6. This high-energy feature in the loss function can be related to the presence in $\mathrm{Im}[\epsilon]$ obtained from the full calculation of a broad peak at energies higher than 15.5 eV as seen in the inset of the middle panel of Fig. 3. In general, our calculated $\mathrm{Im}[\epsilon]$ is notably higher than that obtained experimentally in

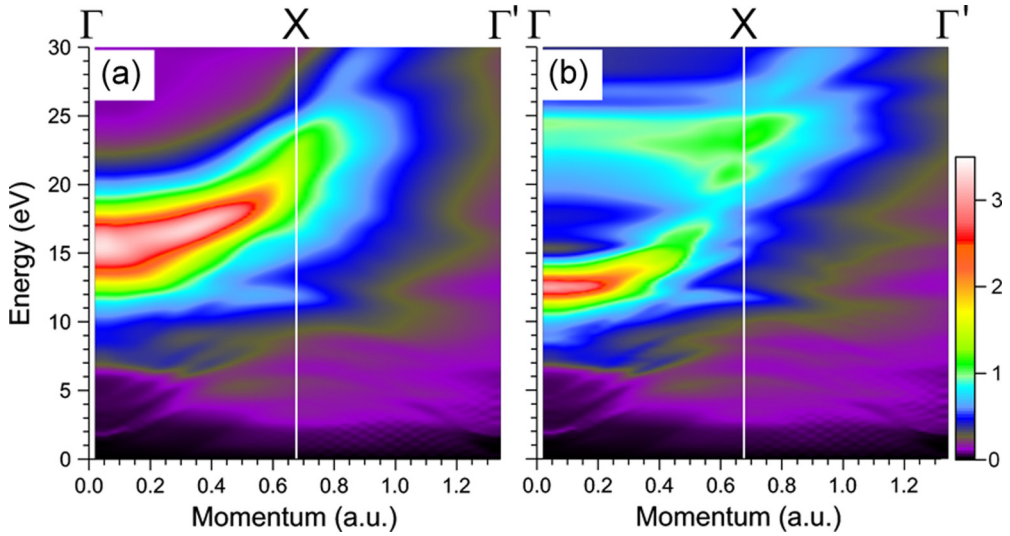

FIG. 4. (Color online) Energy-loss function evaluated (a) without and (b) with inclusion of the semicore 5*d* states for momentum transfers along the Γ-*X* symmetry direction. Calculations were performed taking into account the SO coupling, LFEs, and the TDLDA XC kernel.

the 15.5 to 18.5 eV energy interval. Moreover, in the inset of the middle panel of Fig. 3 it is clearly seen that our curve for Im[ϵ] exceeds the all-electron one over a wide energy interval up to 24.5 eV. This may point to some overestimation of the transition matrix elements based on the pseudopotential wave functions used for the description of the localized 5*d* semicore states in the pseudopotential calculations.

A downward shift of the plasmonic peak in the energy-loss function upon inclusion of 5*d* bands into a valence set is accompanied by a strong reduction of its linewidth. At first glance it looks rather strange since, in the inset of the middle panel of Fig. 3, the Im[ϵ] (the green dash-dot-dot line) at 16 eV is smaller than that in the black solid line at 12.5, which would suggest an opposite trend. However, one should recall that the width of the plasmonic peak is also inversely proportional to $d\mathrm{Re}[\epsilon(\omega)]/d\omega$. Indeed, in the inset of the top panel of Fig. 3 one can see that Re[ϵ] shown by a solid line disperses much faster at 12.5 eV than the green dash-dot-dot line at 15 eV. The competition of these two factors leads to a significant reduction of the plasmon peak width (or its lifetime increase).

Concerning the details of the broad features present in the energy-loss function at energies above 15 eV, there is some disagreement between our theoretical results and those of Werner *et al.* [63] and between both calculations and the experimental data of Werner *et al.* [63]. Thus, the calculations overestimate the energy-loss function at energies below 20 eV. At all energies above 20 eV the calculations of Ref. [63] underestimate the spectral weight. In the present calculations a wide peak is located at 24.5 eV, i.e., at an energy around 3 eV higher than in the experimental curve although its strength is comparable. One can also see that the black solid line contains another peak at energy of 27 eV whereas the experimental spectrum presents a rather broad peak located around 25.2 eV. Finally, in the reflectance measurements of Ashton and Green [66], peaks in Im[ϵ^{-1}] at 12.7 and 21.5 eV were reported, which are in good agreement with the REELS data of Ref. [63]. One additional peak was also reported at 18.7 eV, which is not observed in the REELS data. However, it can be compared with some hump in our energy-loss function in this energy region.

B. Dispersion of excitations

Figure 4 presents the energy-loss function as a function of energy and momentum transfer along the Γ-*X* symmetry direction obtained without [Fig. 4(a)] and with [Fig. 4(b)] inclusion of the semicore 5*d* states in the valence configuration. Calculations were performed by taking into account the SO coupling, the LFEs, and the TDLDA XC kernel. From the comparison of these two panels one can observe over the extended momentum-transfer region how incorporation of the semicore 5*d* electrons in the calculations reduces the bulk Pb plasmon energy in the long-wavelength limit by roughly 3 eV. This downward shift of the plasmon dispersing peak also shortens significantly the momentum-transfer range in which the plasmon is well defined. These remarkable effects caused by inclusion of the semicore 5*d* states on the Pb plasmon dispersion are found to be essentially independent of the level of description of both XC effects (RPA or TDLDA) and inclusion of LFEs, although, as will be shown below, the SO interaction has some effect in the reduction of the bulk plasmon energy at low momentum transfers. Additionally, in Fig. 4(b) some enhancement in the energy-loss function in the 20 to 26 eV energy range at q smaller than 0.7 a.u. can be appreciated.

In order to understand the origin of the modifications in the loss function seen in Fig. 4 upon inclusion of the 5*d* semicore states we compare in Fig. 5 the imaginary part of the noninteracting density response function $\chi^0(q,\omega)$ as a function of energy and momentum transfer along the same symmetry direction evaluated without [Fig. 5(a)] and with [Fig. 5(b)] inclusion of the 5*d* semicore electrons in the valence configuration. From Fig. 5 it is clear that the downward shift of the main bulk plasmon peak reduces the critical momentum transfer q_c at which the plasmon branch enters the electron-hole pair continuum, as shown by arrows in both cases. Upon entering this continuum the plasmon

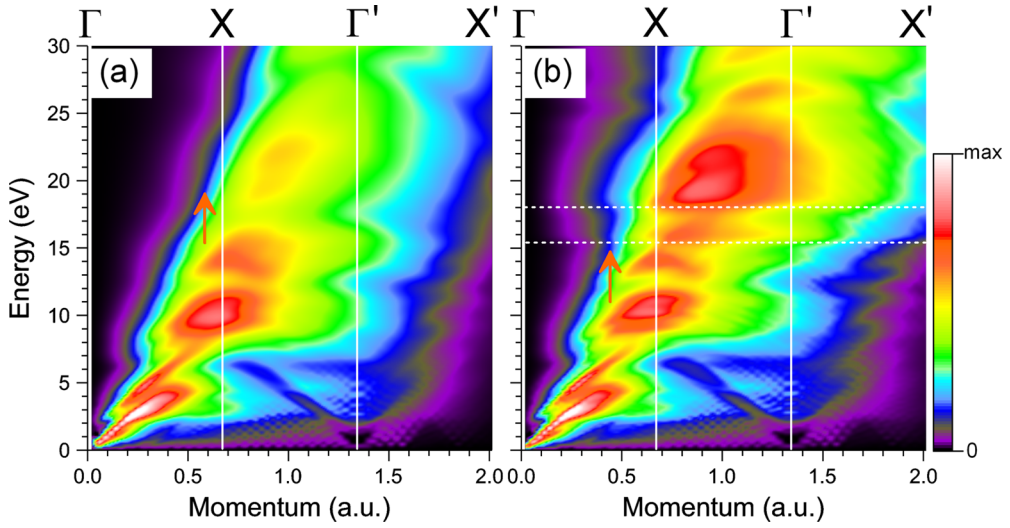

FIG. 5. (Color online) Imaginary part of the noninteracting density-response function, $\mathrm{Im}[\chi^0(\mathbf{q},\omega)]$, for momentum transfers along the Γ-X direction with the SO included and (a) excluding and (b) including the semicore $5d$ electrons in the valence configuration. Vertical arrows show the position of q_c where the plasmon dispersion curve enters the region with increased number of electron-hole pairs. Horizontal dotted lines show the energy thresholds for interband transitions involving the energy bands originated from the $5d_{5/2}$ and $5d_{3/2}$ states. Vertical arrows point to regions where the plasmon peak enters the electron-hole pair continuum.

excitation quickly ceases to be a well-defined excitation due to efficient decay into electron-hole pairs [1]. In panel Fig. 5(b) one can note the presence in $\mathrm{Im}[\chi^0(\mathbf{q},\omega)]$ of two thresholds for interband transitions between the strongly SO-split $5d_{5/2}$ and $5d_{3/2}$ states and the lowest unoccupied energy bands, as marked by horizontal dotted lines. Above these energies $\mathrm{Im}[\epsilon]$ is notably enhanced due to such interband transitions. Hence, the above-mentioned enhancement at energies above 20 eV in the energy-loss function of Fig. 4(b) can be explained by the increase of $\mathrm{Im}[\epsilon]$ at $\omega \gtrsim 15$ eV (Fig. 5) caused by the interband transitions from these $5d$ bands to the unoccupied states.

V. GENERAL RESULTS

As was demonstrated in Fig. 4, incorporation of the semicore $5d$ electrons in the calculation of the dielectric response of bulk Pb leads to significant modifications in the energy-loss function. In particular, instead of finding a bulk plasmon peak with a full width at half maximum (FWHM) of around 4 eV and exhibiting a clear upward dispersion, the inclusion of the semicore states produces a downward plasmon-peak shift of about 3.5 eV, a flatter dispersion, a smaller q region where the plasmon is well defined, and a significant reduction of its peak linewidth up to $\sim$1.5 eV. Such strong impact of the interband transitions involving the $5d$ electrons is found regardless of the momentum-transfer direction, inclusion or not of the SO coupling and LFEs, and of the type of the XC kernel employed. Thus, the effect of inclusion of the TDLDA kernel is limited by a modest increase of the loss function amplitude without notable variation of its shape. For concreteness, all the results reported in the present work were obtained using the TDLDA kernel. Looking at Fig. 6 one can observe that the calculated loss function at large momentum transfers is dominated, except the weak peaks denoted by dashed and dotted lines, by a single high-energy broad peak. This observation suggests that lead might be a more suitable candidate than Be and Al for observation [67–70] at low energies of the multipair and excitonic effects which were previously discussed for simple metals [71].

Although the major effect on the formation of collective electronic excitations in bulk lead in the energy region of interest here comes from the semicore $5d$ states, additional ingredients also play a role. In order to demonstrate the relative strength of each of them, in Fig. 6 we show the collection of different results for the evaluated energy-loss function as a function of energy and momentum transfer along the three high-symmetry directions. In particular, the left column stands for the energy-loss function obtained with the inclusion of SO and LFE, while the SO interaction (LFE) was excluded from the calculations corresponding to the right (middle) column.

As seen in Fig. 6, switching on the LFEs (compare the left and middle columns) results in a spectral weight transfer from the broad peak, located in the $19 \lesssim \omega \lesssim 24$ eV energy interval [as an example, labeled by B in Fig. 6(g)] and formed by the interband transitions from the $5d$ electrons, to the bulk plasmon peak at $\omega \simeq 12-13$ eV [as en example, one labeled by A in Fig. 6(g)]. Moreover, the inclusion of the LFEs increases the bulk plasmon peak intensity over a wide range of q, as can also be appreciated in Fig. 7 where $\mathrm{Im}[\epsilon^{-1}(q,\omega)]$ is reported as a function of ω at certain q along Γ-L. In general, one can conclude that, in the extended energy range, the LFEs produce transmission of the spectral weight from the upper energy feature to the main plasmon peak in any direction similar to what was obtained in the low-energy domain [31], contributing to the shape of the bulk plasmon as the most prominent feature in the excitation spectrum.

On the other hand, by comparing the right and left columns of Fig. 6, one can deduce that the SO interaction increases the intensity of the higher-energy peak [as an example, one labeled by B in Fig. 6(g)] related to the interband transitions involving

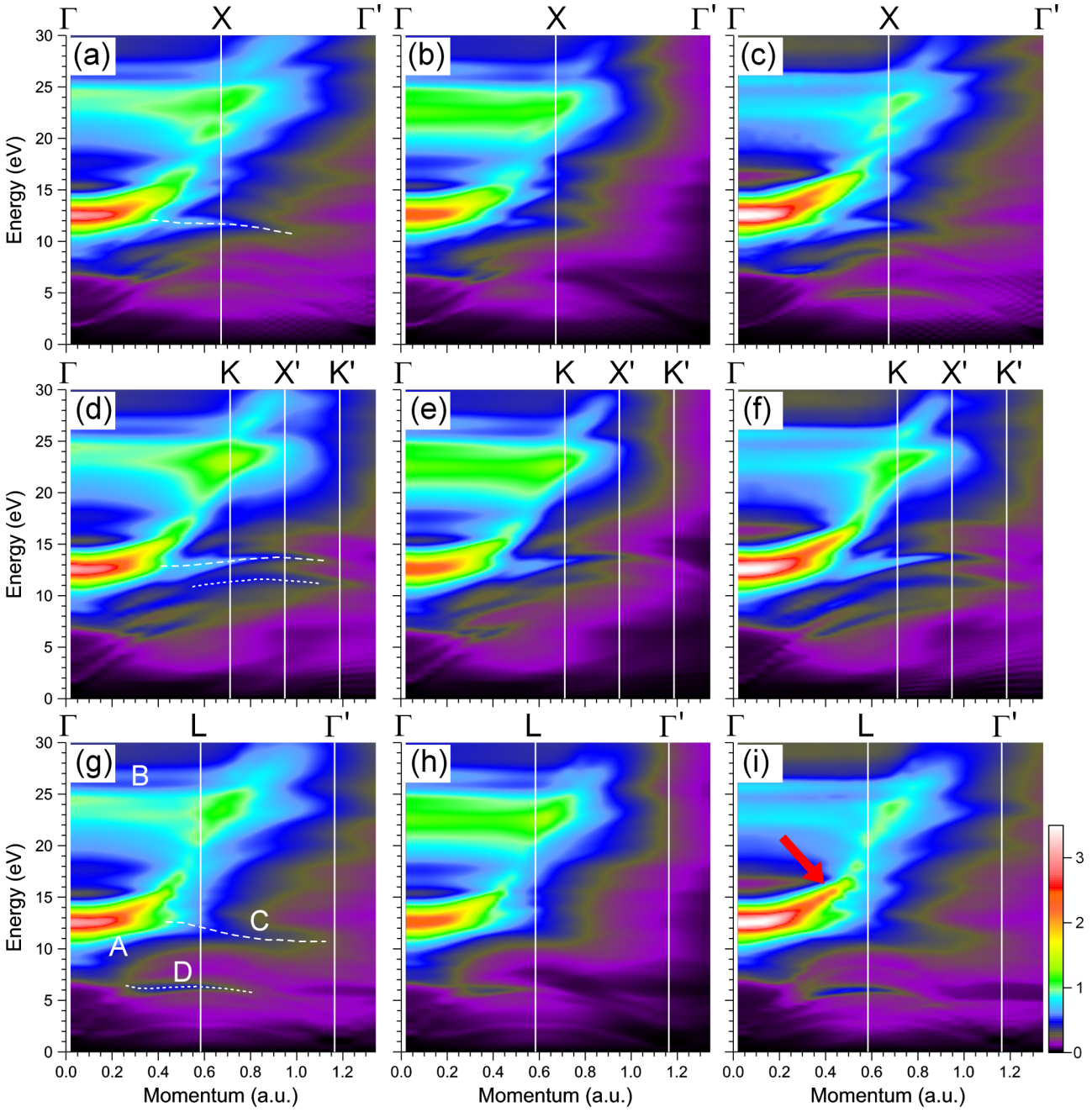

FIG. 6. (Color online) Energy-loss function surfaces calculated with the semicore 5*d* states included in the valence configuration. The upper, middle, and bottom rows correspond to the results with **q** along Γ-*X*, Γ-*K*, and Γ-*L* symmetry directions, respectively. High-symmetry points are marked by thin white vertical lines. The left column stands for $\mathrm{Im}[\epsilon^{-1}_{0,0}(\mathbf{q},\omega)]$ obtained with the SO coupling and LFE included, whereas SO coupling (LFE) was excluded from the calculations corresponding to the right (middle) column. See text for the meaning of the symbols in panels (g) and (i).

the semicore 5*d* states. More importantly, the SO coupling reduces the plasmon peak at $q \lesssim 0.35$ a.u. and shortens the momentum-transfer range in which the bulk plasmon is well defined, depleting its intensity in the $0.35 \lesssim q \lesssim 0.5$ a.u. range [as pointed out by the red arrow in Fig. 6(i)].

This notable SO effect is clearly observed in the cuts of $\mathrm{Im}[\epsilon^{-1}_{0,0}(\mathbf{q},\omega)]$ plotted in Fig. 7(b) where the bulk plasmon peak is still well defined in the scalar-relativistic calculation while it is significantly reduced in the full calculation. Additionally, as seen in Fig. 7(a) the inclusion of the SO coupling leads to reduction of the plasmon peak linewidth by about 0.5 eV.

Comparison of the left panels of Fig. 6 demonstrates that, in general, the excitation spectrum in Pb only slightly depends on the momentum-transfer direction. At small q the spectrum is essentially the same in all directions. Some differences can be observed at $q \gtrsim 0.2$ a.u. where several weak peaks are highlighted by dashed and dotted lines. Among them the most pronounced ones are shown by dashed lines as the peak C dispersing downward upon the momentum increase, and those

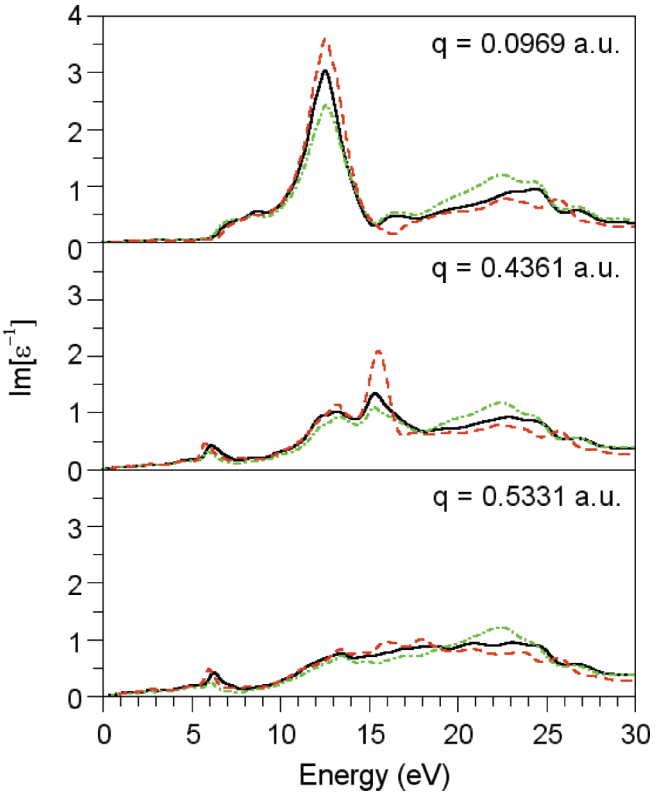

FIG. 7. (Color online) Calculated energy-loss function at three different values of q along Γ-L. Black solid, red dashed and green dashed-dotted curves stand for the results obtained with SO and LFE included, SO coupling excluded, and LFE ignored, respectively.

with a small spectral weight indicated by dotted lines like the peak D presenting almost no dispersion.

VI. CONCLUSIONS

Semicore 5*d* states are found to play a crucial role in the establishment of high-energy dielectric properties of bulk Pb. In particular, the interband transitions involving the corresponding bands strongly promote a downward shift of the plasmon energy by ∼3.5 eV down to 12.5 eV, in close agreement with a recent energy-loss experiment. This shift is accompanied by a reduction of the maximal momentum transfer up to 0.4 a.u. defining the region where the plasmon can be considered as a well-defined excitation, together with a reduction of the plasmon peak linewidth. These transitions also reduce the dispersion of the plasmon and, additionally, produce a wide peak in the energy-loss function in the 20 to 25 eV interval.

Once the 5*d* electrons are explicitly incorporated in the dielectric response calculations, the energy-loss function is shaped by the competition between local-field effects and spin-orbit interaction. In particular, the SO coupling shortens the momentum-transfer range in which the bulk plasmon is well defined, while enhancing intensity of the 20 to 25 eV broad peak. On the contrary, the influence of LFE is limited to the enhancement of the plasmon peak intensity and the reduction of the high-energy broad interband peak intensity.

In the small-momentum-transfer regime it is found that the excitation spectrum in Pb is rather isotropic. Some anisotropy is observed at finite momentum transfers; however, it represents a minor effect.

ACKNOWLEDGMENTS

We acknowledge financial support from the Spanish MINECO (Grant No. FIS2013-48286-C2-1-P), the Departamento de Educación del Gobierno Vasco, and the University of the Basque Country (Grant No. GIC07-IT-366-07).

[1] D. Pines and P. Nozières, *The Theory of Quantum Liquids* (Benjamin, New York, 1966).
[2] M. J. Stott and E. Zaremba, Phys. Rev. A **21**, 12 (1980).
[3] J. F. Dobson and J. H. Rose, J. Phys. C: Solid State Phys. **15**, 7429 (1982).
[4] E. K. U. Gross and W. Kohn, Phys. Rev. Lett. **55**, 2850 (1985).
[5] C. F. Richardson and N. W. Ashcroft, Phys. Rev. B **50**, 8170 (1994).
[6] G. Vignale and W. Kohn, Phys. Rev. Lett. **77**, 2037 (1996).
[7] M. Lein, E. K. U. Gross, and J. P. Perdew, Phys. Rev. B **61**, 13431 (2000).
[8] H.-C. Weissker, J. Serrano, S. Huotari, F. Bruneval, F. Sottile, G. Monaco, M. Krisch, V. Olevano, and L. Reining, Phys. Rev. Lett. **97**, 237602 (2006).
[9] I. G. Gurtubay, J. M. Pitarke, W. Ku, A. G. Eguiluz, B. C. Larson, J. Tischler, P. Zschack, and K. D. Finkelstein, Phys. Rev. B **72**, 125117 (2005).
[10] A. A. Quong and A. G. Eguiluz, Phys. Rev. Lett. **70**, 3955 (1993).
[11] S. L. Adler, Phys. Rev. **126**, 413 (1962).
[12] N. Wiser, Phys. Rev. **129**, 62 (1963).
[13] E. E. Krasovskii and W. Schattke, Phys. Rev. B **60**, R16251 (1999).
[14] E. E. Krasovskii and W. Schattke, Phys. Rev. B **63**, 235112 (2001).
[15] V. P. Zhukov, V. M. Silkin, E. V. Chulkov, and P. M. Echenique, Phys. Rev. B **64**, 180507(R) (2001).
[16] W. Ku, W. E. Pickett, R. T. Scalettar, and A. G. Eguiluz, Phys. Rev. Lett. **88**, 057001 (2002).
[17] Y. Q. Cai, P. C. Chow, O. D. Restrepo, Y. Takano, K. Togano, H. Kito, H. Ishii, C. C. Chen, K. S. Liang, C. T. Chen, S. Tsuda, S. Shin, C. C. Kao, W. Ku, and A. G. Eguiluz, Phys. Rev. Lett. **97**, 176402 (2006).
[18] R. Hambach, C. Giorgetti, F. Sottile, L. Reining, N. Hiraoka, Y. Q. Cai, A. G. Marinopoulos, and F. Bechstedt, Phys. Rev. Lett. **101**, 266406 (2008).
[19] I. Errea, A. Rodriguez-Prieto, B. Rousseau, V. M. Silkin, and A. Bergara, Phys. Rev. B **81**, 205105 (2010).
[20] M. N. Faraggi, A. Arnau, and V. M. Silkin, Phys. Rev. B **86**, 035115 (2012).
[21] P. Cudazzo, M. Gatti, and A. Rubio, Phys. Rev. B **86**, 075121 (2012).
[22] S. V. Eremeev *et al.*, Nat. Commun. **3**, 635 (2012).

[23] V. Chis, I. Yu. Sklyadneva, K. A. Kokh, V. A. Volodin, O. E. Tereshchenko, and E. V. Chulkov, Phys. Rev. B **86**, 174304 (2012).
[24] X. Gonze, J.-P. Michenaud, and J.-P. Vigneron, Phys. Rev. B **41**, 11827 (1990).
[25] L. E. Díaz-Sánchez, A. H. Romero, and X. Gonze, Phys. Rev. B **76**, 104302 (2007).
[26] M. J. Verstraete, M. Torrent, F. Jollet, G. Zérah, and X. Gonze, Phys. Rev. B **78**, 045119 (2008).
[27] R. Heid, K.-P. Bohnen, I. Yu. Sklyadneva, and E. V. Chulkov, Phys. Rev. B **81**, 174527 (2010).
[28] X. Zubizarreta, V. M. Silkin, and E. V. Chulkov, Phys. Rev. B **84**, 115144 (2011).
[29] S. V. Eremeev, I. A. Nechaev, Yu. M. Koroteev, P. M. Echenique, and E. V. Chulkov, Phys. Rev. Lett. **108**, 246802 (2012).
[30] I. Yu. Sklyadneva, R. Heid, K.-P. Bohnen, V. Chis, V. A. Volodin, K. A. Kokh, O. E. Tereshchenko, P. M. Echenique, and E. V. Chulkov, Phys. Rev. B **86**, 094302 (2012).
[31] X. Zubizarreta, V. M. Silkin, and E. V. Chulkov, Phys. Rev. B **87**, 115112 (2013).
[32] K. Glantschnig and C. Ambrosch-Draxl, New J. Phys. **12**, 103048 (2010).
[33] V. M. Silkin, A. Balassis, P. M. Echenique, and E. V. Chulkov, Phys. Rev. B **80**, 054521 (2009).
[34] V. M. Silkin, I. P. Chernov, Yu. M. Koroteev, and E. V. Chulkov, Phys. Rev. B **80**, 245114 (2009).
[35] J. P. Echeverry, E. V. Chulkov, P. M. Echenique, and V. M. Silkin, Phys. Rev. B **85**, 205135 (2012).
[36] H. Ehrenreich and H. R. Philipp, Phys. Rev. **128**, 1622 (1962).
[37] R. M. Morgan and D. W. Lynch, Phys. Rev. **172**, 628 (1968).
[38] A. vom Felde, J. Fink, Th. Büche, B. Scheerer, and N. Nücker, Europhys. Lett. **4**, 1037 (1987).
[39] A. vom Felde, J. Sprösser-Prou, and J. Fink, Phys. Rev. B **40**, 10181 (1989).
[40] F. Aryasetiawan and K. Karlsson, Phys. Rev. Lett. **73**, 1679 (1994).
[41] A. Fleszar, R. Stumpf, and A. G. Eguiluz, Phys. Rev. B **55**, 2068 (1997).
[42] F. Roth, A. König, C. Kramberger, T. Pichler, B. Büchner, and M. Knupfer, Europhys. Lett. **102**, 17001 (2013).
[43] R. Schuster, R. Kraus, M. Knupfer, H. Berger, and B. Büchner, Phys. Rev. B **79**, 045134 (2009).
[44] J. van Wezel, R. Schuster, A. König, M. Knupfer, J. van den Brink, H. Berger, and B. Büchner, Phys. Rev. Lett. **107**, 176404 (2011).
[45] A. König, R. Schuster, M. Knupfer, B. Büchner, and H. Berger, Phys. Rev. B **87**, 195119 (2013).
[46] S. Kaltenborn and H. C. Schneider, Phys. Rev. B **88**, 045124 (2013).
[47] S. G. Louie, S. Froyen, and M. L. Cohen, Phys. Rev. B **26**, 1738 (1982).
[48] B. E. Tegner and G. J. Ackland, Comput. Mater. Sci. **52**, 2 (2012).
[49] S. Huotari, M. Cazzaniga, H.-C. Weissker, T. Pylkkänen, H. Müller, L. Reining, G. Onida, and G. Monaco, Phys. Rev. B **84**, 075108 (2011).
[50] M. Cazzaniga, H.-C. Weissker, S. Huotari, T. Pylkkänen, P. Salvestrini, G. Monaco, G. Onida, and L. Reining, Phys. Rev. B **84**, 075109 (2011).
[51] E. Runge and E. K. U. Gross, Phys. Rev. Lett. **52**, 997 (1984).
[52] M. Petersilka, U. J. Gossmann, and E. K. U. Gross, Phys. Rev. Lett. **76**, 1212 (1996).
[53] G. D. Mahan, *Many Particle Physics* (Plenum, New York, 1981).
[54] E. K. U. Gross, J. F. Dobson, and M. Petersilka, in *Density Functional Theory II*, edited by R. F. Nalewajski (Springer, Berlin, 1996).
[55] M. Corradini, R. Del Sole, G. Onida, and M. Palummo, Phys. Rev. B **57**, 14569 (1998).
[56] F. Aryasetiawan and O. Gunnarsson, Phys. Rev. B **49**, 16214 (1994).
[57] F. Aryasetiawan, in *Strong Coulomb Correlations in Electronic Structure Calculations*, edited by V. I. Anisimov (Gordon and Beach, Singapore, 2001).
[58] G. B. Bachelet, D. R. Hamann, and M. Schlüter, Phys. Rev. B **26**, 4199 (1982).
[59] J. P. Perdew and A. Zunger, Phys. Rev. B **23**, 5048 (1981).
[60] D. M. Ceperley and B. J. Alder, Phys. Rev. Lett. **45**, 566 (1980).
[61] H. J. Monkhorst and J. D. Pack, Phys. Rev. B **13**, 5188 (1976).
[62] G. Jézéquel and I. Pollini, Phys. Rev. B **41**, 1327 (1990).
[63] W. S. M. Werner, K. Glantschnig, and C. Ambrosch-Draxl, J. Phys. Chem. Ref. Data **38**, 1013 (2009).
[64] C. Ambrosch-Draxl and J. O. Sofo, Comput. Phys. Commun. **175**, 1 (2006).
[65] E. A. Bakulin, L. A. Balabanov, M. M. Bredov, and E. V. Stepin, Fizika Tverd. Tela **16**, 2568 (1974) [Sov. Phys. Solid State **16**, 1670 (1975)].
[66] A. M. Ashton and G. W. Green, J. Phys. F: Met. Phys. **3**, 179 (1973).
[67] P. M. Platzman and P. Eisenberger, Phys. Rev. Lett. **33**, 152 (1974).
[68] P. M. Platzman, E. D. Isaacs, H. Williams, P. Zschack, and G. E. Ice, Phys. Rev. B **46**, 12943 (1992).
[69] W. Schülke, H. Schulte-Schrepping, and J. R. Schmitz, Phys. Rev. B **47**, 12426 (1993).
[70] B. C. Larson, J. Z. Tischler, E. D. Isaacs, P. Zschack, A. Fleszar, and A. G. Eguiluz, Phys. Rev. Lett. **77**, 1346 (1996).
[71] Y. Takada and H. Yasuhara, Phys. Rev. Lett. **89**, 216402 (2002).